Journal of Materials Chemistry A

Accepted Manuscript

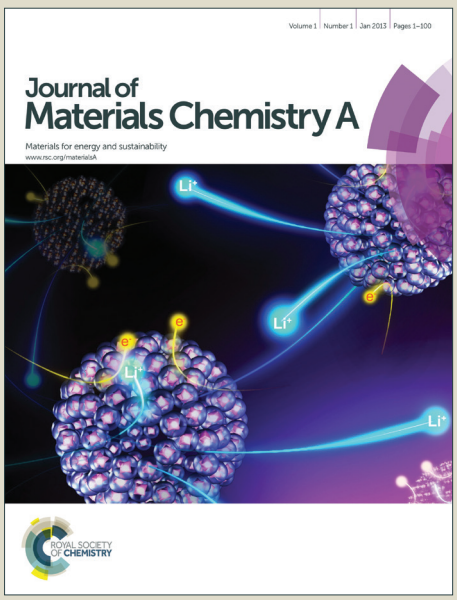

ROYAL SOCIETY OF CHEMISTRY

www.rsc.org/materialsA

Interaction of Substituted Poly(phenyleneethynylene)s with Ligand-Stabilized CdS Nanoparticles

by

Hua Liu[#], Matthew Espe[※], David A. Modarelli [※], Eduardo Arias[§], Ivana Moggio[§], Ronald F. Ziolo[§], Hendrik Heinz[#*]

[#] Department of Polymer Engineering, University of Akron, Akron, OH 44325, USA

[※] Department of Chemistry, University of Akron, Akron, OH 44325, USA

[§] Centro de Investigación en Quimica Aplicada (CIQA), 25294 Saltillo, Coahuila, México

* Corresponding author: hendrik.heinz@uakron.edu

Abstract

The interfacial region between surface-modified semiconducting nanoparticles and polymers remains difficult to characterize experimentally in atomic resolution and contributes to the limited efficiency of hybrid photovoltaic cells and luminescent devices. Therefore, molecular dynamics simulation was employed to investigate the structure of cadmium sulfide nanoparticles capped with 3-mercaptopropyltrimethoxysilane (MPS) in contact with four substituted poly(phenyleneethynylene)s using a new force field for CdS and the polymer consistent force field. The results show that polymers with long alkyl side chains tend to wrap around the nanoparticles, reduce backbone bending, and polymer diffusion. The absence of alkyl side chains decreases the distance of conjugated backbones from the surface. Differences in the preferred location of functional groups of the polymers on the nanoparticle surface and of covalent versus non-covalent bonding were also monitored. Polymers containing terminal hydroxyl groups on alkyl side chains approach the surfactant corona and the core of the CdS-MPS nanoparticles. Close contact supports the formation of silyl ether cross-links although the interfacial structure upon bond formation remains similar to that of the non-covalently attached polymers. Ester groups bound to aromatic rings in the poly(phenylene ethynylene) backbone did not closely approach the nanoparticle surface. The results are a first step to understand nanoparticle-polymer interfaces at length scales of 10 nm and explore correlations with photovoltaic performance.

1. Introduction

Cadmium sulfide is a II-VI semiconductor that exhibits characteristic size-dependent luminescent properties at the nanometer scale (quantum dots).[1-3] Owed to such optoelectronic properties, CdS nanoparticles (NPs) find applications in LEDs, photovoltaic devices, sensors, fluorescent labels, infrared-active windows, and environmental detection devices.[4, 5] As a result of the small size, CdS nanoparticles have a high specific surface energy and aggregate into large clusters that can diminish their utility as a nanoscale probe. Surface modification enables better integration and distribution in polymer matrices.[6-10] In particular, the performance of hybrid solar cells may be increased by harnessing properties of a semiconductor polymer host with those of the quantum dots via interaction through a large interfacial area. Tests of solar devices based on CdS NP-polymer composites have been reported.[8, 9, 11-14]

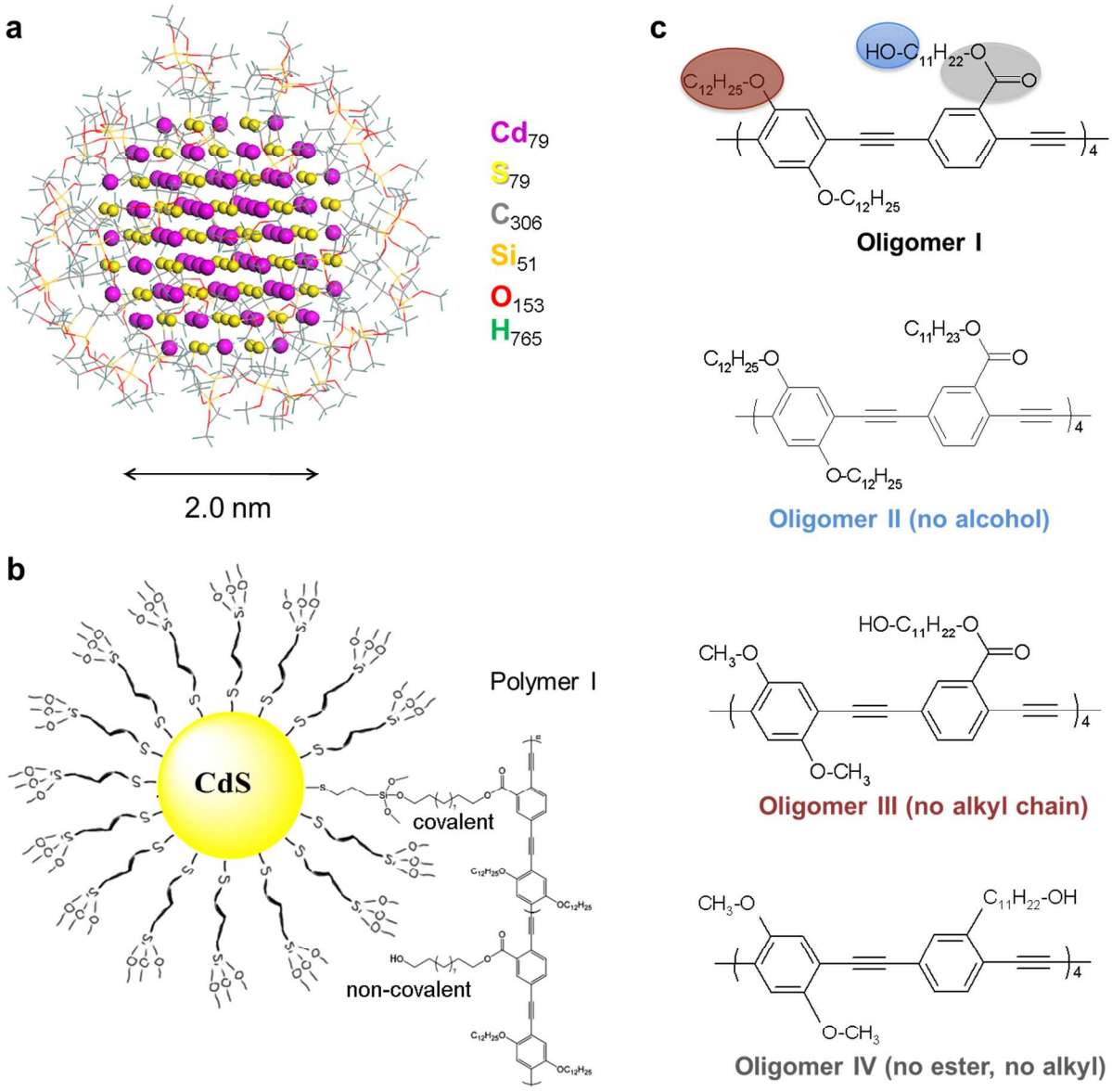

Figure 1. Modified CdS nanoparticles and polymers investigated. (a) Equilibrium model of a CdS nanoparticle core modified with a 3-mercaptopropyltrimethoxysilane corona according to molecular dynamics simulation. Atoms are shown in sphere and line style, respectively. The diameter of the core is 2 nm and 51 surfactants are attached via superficial sulfur as an approximation. (b) Possible covalent and non-covalent attachment of polymer I through formation of silyl ether bonds with the ligand shell. (c) Parent oligomer I and a series of oligomers derived by modification of functional groups employed in simulations.

The main components of inorganic-organic photovoltaic devices are semiconducting nanoparticles, stabilizing ligands, and polymers (Figure 1). ω-Trimethoxysilylalkyl groups have been widely used as a capping agents on the surface of CdS nanoparticles to achieve compatibility (Figure 1a).[15-20] In order to disperse CdS nanoparticles in a polymer host, the first step involves the synthesis of CdS NPs covered by a layer of thiol derivatives, as in the case of 3-mercaptopropyltrimethoxysilane (MPS) (Scheme 1 and ESI):

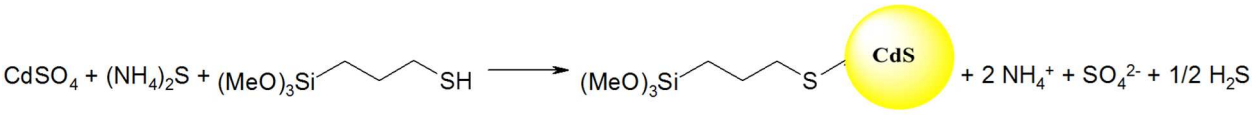

(Scheme 1)

The mechanism of formation of the ligand-stabilized NPs and the resulting interfacial structure has been the subject of several investigations, although some uncertainty remains due to mostly indirect evidence by elemental analysis, XPS, and NMR spectroscopy.[21-27] Thermodynamically, the stoichiometric formation of a CdS core appears likely as a first step, followed by partial substitution of superficial sulfide by twice the amount of thiolate (see section S1 in the ESI for details). This process can result in various degrees of thiol surface coverage and structural heterogeneity in agreement with NMR measurements.[10, 22, 26-28] A simplified model with high surface coverage is assumed here in agreement with available data, and more detailed structures can be explored as further information from experimental investigations becomes available (Figure 1a).[27]

The MPS-capped CdS sulfide nanoparticles can then be immersed in polymer matrices through non-covalent polar and van-der-Waals interactions, as well as through cross-links with certain functional groups (Figure 1b).[10] The polymers of interest were poly(2,5-didodecanoxy-1,4-phenyleneethynylene-2-(11-hydroxyundecyloxycarbonyl)-1,4-phenyleneethynylene) and three derivatives (Figure 1c).[29-31] Oligomers of 1500 to 3000 g/mol molecular weight were chosen that represent the lower range of molecular weight in synthesis[29-31] and allow sufficient conformation sampling in the simulation. The parent oligomer I and the derivatives II-IV differ in the presence of functional groups, such as the hydroxyl groups (II), the alkyl side chains in one of the phenylene rings (III), and the absence of the ester group in one phenylene ring (IV).

The structure of nanoparticle-ligand-monomer interfaces has been characterized using ^{113}Cd, ^{29}Si and ^{13}C NMR, ^{13}C-^{1}H HETCOR, UV, and IR techniques[7, 10] although nanoparticle-polymer interfaces are difficult to monitor by scattering, spectroscopy, and analysis of reaction products. Indications of chemical reactivity of the MPS-capped CdS nanoparticles towards the polymers were previously noted,[10] and some silyl ether links between superficial trimethoxysilyl groups of MPS and ω-alcohol groups of pendant polymer side chains may be formed (Figure 1b). The aim of this study is to better explain the structure and dynamics of the non-covalently bound polymers with respect to the ligand shell and core of the nanoparticles using molecular dynamics simulations and analyze the likelihood of the formation of cross-links (Figure 1c).

2. Simulation Details

The model of the CdS nanoparticle core was chosen according to experimental observations with a diameter of 2.0 nm.[10, 16] Precipitation of CdS from $CdSO_4$ produces cubic β-CdS with zincblende structure (also called Hawleyite) rather than hexagonal α-CdS with wurtzite structure.[1-3, 32-34] The model of the nanoparticle was thus constructed starting with a model of bulk β-CdS according to X-ray data, followed by application of a spherical cutoff of 1.0 nm centered at a Cd^{2+} ion, preserving 1:1 stoichiometry and charge neutrality.[1, 32, 33] The resulting near-spherical symmetry is consistent with TEM observations and the surface is "atomically discretized" (Figure 1a).[8] Visual inspection of β-CdS versus α-CdS also indicated that the actual structure may have limited impact on the polymer interface because local coordination environments are similar and shielded by a 0.0 to 0.5 nm thin layer of organic surfactants.[35-37]

A force field for CdS was developed to simulate the nanoparticle and the interfaces using the INTERFACE approach.[38] The energy expression consists of a Coulomb potential and a 9-6 Lennard Jones (LJ) potential. Two atom types for Cd^{2+} and S^{2-} were defined with atomic charges of +1.0e and -1.0e (±0.1e), consistent with the extended Born model and similar semi-ionic compounds.[39] LJ parameters represent ionic radii and polarizability.[38, 40, 41] Crystal geometry and lattice parameters are reproduced in excellent agreement of 0.1% with experiment during NPT molecular dynamics. The parameters are integrated into the polymer consistent force field (PCFF),[42, 43] the INTERFACE force field,[38] and are extensible to other quantum dots such as (Zn, S)(S, Se, Te) (see details of procedures, parameters, and validation in section S2 in the ESI).

The nanoparticle diameter increases from 2 nm up to approximately 3.0 nm upon capping with 3-mercaptopropyltrimethoxysilane (MPS). Most sulfide ions are located on the nanoparticle

surface (51 out of 79) and these superficial sulfide ions were modified as covalent links with MPS for simplicity (Figure 1a). The atomic charge on these bridging sulfide atoms was chosen as -1.065e to maintain overall charge neutrality. The surface saturation with ligands was comparatively high (λ=0.85, 4.5 ligands per nm^2),[27, 28] corresponding to a net formula of the model CdS-MPS nanoparticles of $Cd_{79}S_{79}C_{306}Si_{51}H_{765}O_{153}$. Models with different stoichiometry of the ligand shell, disorder of surface groups, and variations in surface coverage can be explored in future work (see section S1 in the ESI for details and discussion).[10, 22, 26, 27]

The polyphenyleneethynylene polymers were represented as oligomers with N = 4 for feasibility in the simulation (Scheme 2 and Figure 1c):

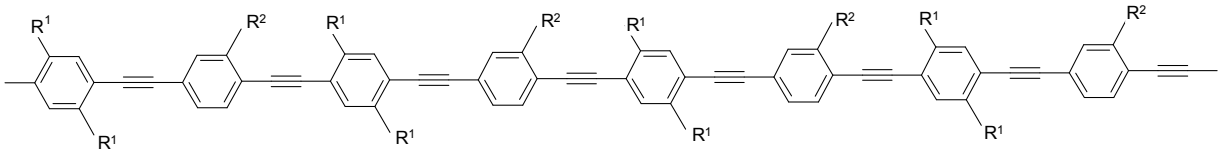

(Scheme 2)

The backbone is rod-like and approximately 5 nm long. Ethynylene and phenylene connector carbon atoms carry small negative and positive charges (±0.0852e) in accordance with electronegativity differences.[44] Force field parameters for the MPS surfactants and the oligomers were assigned according to PCFF, which is known to reproduce properties of alkyl chains, silyl ethers, and conjugated polymers well.[42, 43]

Simulation boxes contained two CdS-MPS nanoparticles with a center-to-center distance fixed at 4.0 nm and 20 oligomers I, II, III, or IV, respectively (Figure 2). The oligomers were non-covalently mixed with the nanoparticles. In addition, one system of covalently bound

oligomer I, with one ether linkage per oligomer to MPS-CdS, was included. The box size was chosen as 8×6.8×6.8 nm^3 in all simulations and contains a significant fraction of vacuum corresponding to total densities of 460, 454, 349, and 333 kg/m^3 for oligomers I, II, III, or IV, respectively. Low oligomer density was necessary to facilitate conformation sampling on the nanoparticle surfaces during accessible time scales. If polymer-vacuum interfaces would be excluded in favor of full equilibrium density, simulations in the NPT ensemble would require larger boxes and simulation times beyond microseconds to achieve conformational equilibrium.

Model building and initial test simulations were carried out using Materials Studio.[42] Final molecular dynamics (MD) simulations were carried out with the program LAMMPS[45] and the PCFF force field[43] extended for CdS. Cadmium and sulfide ions in both nanoparticles were fixed for convenience during all simulations. The simulation protocol involved initially 200 steps of energy minimization to remove atomic close contacts. MD simulation then followed in the NVT ensemble at an increased higher temperature of 473.15 K for 1 ns to enhance conformation sampling via time-temperature equivalence. The temperature was subsequently lowered to 298.15 K to continue MD simulations for 100 ns and record structural and thermodynamic properties. The Verlet integrator, a spherical cutoff for van-der-Waals interactions at 1.2 nm, summation of Coulomb interactions using the PPPM method in medium resolution (10^{-4}), the Nose-Hoover thermostat, and a time step of 1 fs were employed. Analysis involved visual inspection to identify the location of functional groups and the steric likelihood for covalent links between oligomers I-IV and the nanoparticle shell. Then, radial distribution functions of OH groups, ester groups, equilibrium end-to-end lengths of the carbon-based oligomer backbone, mean square displacements of the center of mass of the oligomers, and uncertainties were analyzed. Simplifying assumptions include the use of shorter model oligomers in comparison to

polymers, partial vacuum to accelerate conformation equilibrium, and a uniform grafting density of MPS surfactants at λ=0.85. The accuracy of the force field is unlikely a significant source of error as demonstrated for similar inorganic-organic interfaces[46-49] and extensive conformation sampling was performed. To the best of the authors' knowledge, this work is the first atomistic computational study on *polymer-quantum dot interfaces*.

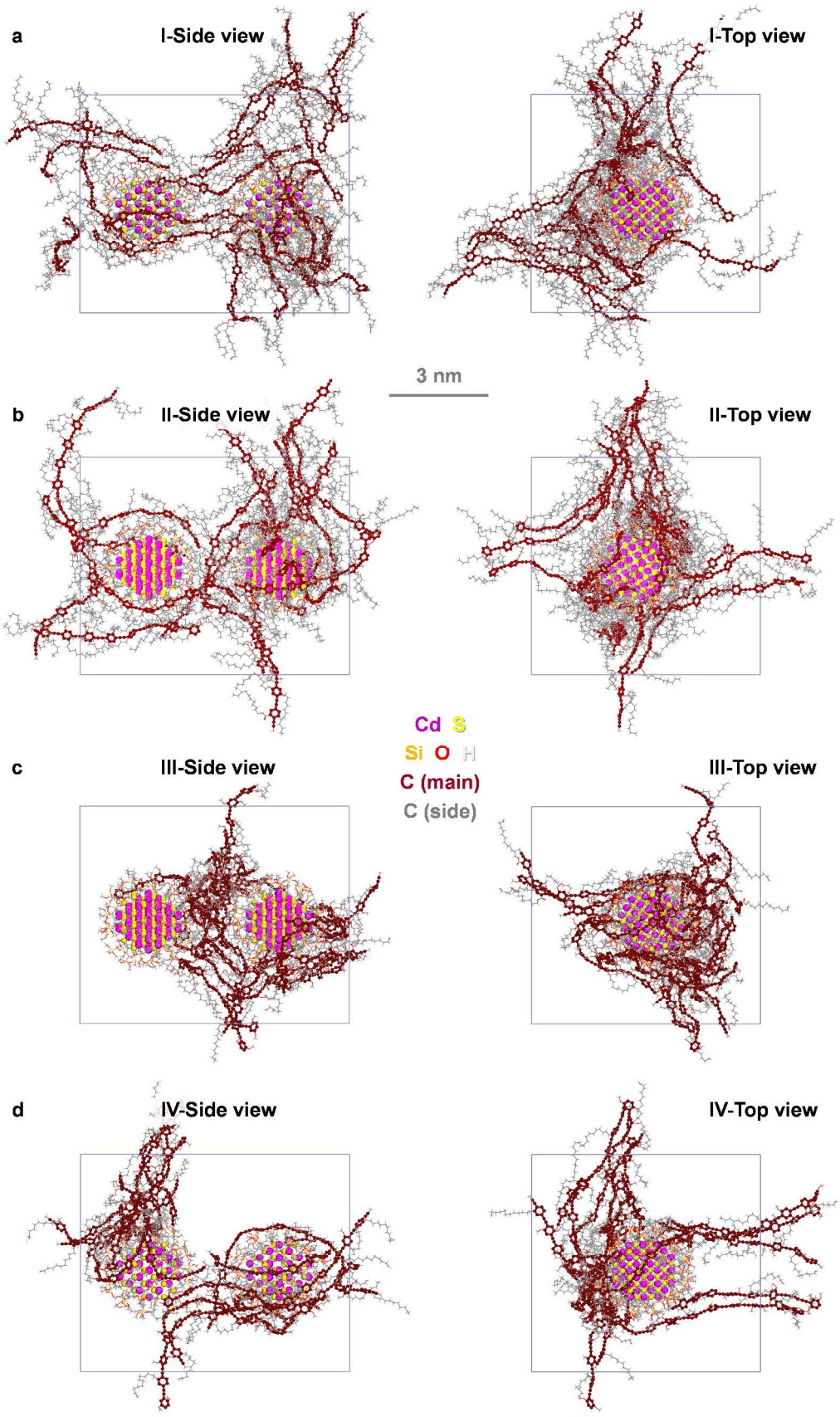

Figure 2. Oligomer assembly on CdS-MPS nanoparticles in molecular dynamics simulation after 100 ns simulation time (backbones highlighted in brown color). The 3D periodic boxes contain two nanoparticles and twenty oligomer chains. (a,b) Flexible side chains in alkyl-rich oligomers I and II tend to wrap onto the nanoparticle surface. (c,d) Alkyl-poor oligomers III and IV exhibit less continuous interfaces with the nanoparticles related to the rod-like nature of the backbone.

3. Results and Discussion

The conformation, position, and morphology of the oligomers in the simulation reflect the stiffness of the conjugated backbone (Figure 2). Packing of the rod-like backbone onto the curved nanoparticle surfaces is difficult and the contact area of the polymer with the nanoparticles largely consists of side chains with conformational flexibility. This effect can be specifically seen for oligomers I and II that contain three side chains per repeat unit (Figure 2a,b) versus oligomers III and IV that contain only one side chain per monomer (Figure 2c,d). Oligomers I and II wrap around the nanoparticle surface, which was also observed when the overall density was reduced to that of oligomers III and IV, while oligomers III and IV do not fully cover portions of the nanoparticle surface. Stiff phenylene ethynylene oligomer backbones without alkyl chains thus have difficulties to surround the nanoparticle surface.

Time-averaged details of the approach of functional groups to the surface were obtained through analysis of radial distribution functions.[50] We choose the Cd atom in the geometric center of the nanoparticles as a reference and computed the radial distribution function of oxygen atoms in hydroxyl groups of the oligomers as well as of carbonyl oxygen atoms in ester groups

of the oligomers as a time average over the second half of the MD trajectory (Figures 3 and 4). The data measure the average distance of the groups from the nanoparticle center. The area under the curve for a given distance interval indicates the local density of OH groups. Visualization and g(r) show that hydroxyl groups in the side chains (Figure 1c) easily approach the nanoparticle core surface for which the MPS surfactant layer leaves open spaces (Figure 3).[28] The peak around 1.0 nm is due to $Cd^{2+}/(S^{2-}/RS^{-}) \cdots$ OH contacts while the peak around 1.2 nm is related to contacts of the OH groups with trimethoxysilyl groups in the ligand shell. The "atomically discretized" surface structure also coarsens the van-der-Waals surface, leading to areas with a nominal radius smaller than 1.0 nm and coordinated OH groups of the oligomers (Figure 3). The relative contribution of both types of contacts, near 1.0 nm and 1.2 nm, is quantified by the relative area under the g(r) curve. Oligomer IV without two extra side chains and without the ester group most closely approaches the nanoparticle core, followed by oligomers III and I. The attraction involves coordinative $Cd^{2+} \cdots$ OH interactions. The approach to $Si(OMe)_3$ groups in the ligand shell is most effective for oligomer III as well as for oligomer IV. Oligomer I with bulkier side chains is sterically disfavored to approach both core and surfactant corona of the nanoparticle and is thus not as effective as oligomers III or IV. As a consequence, a larger portion of hydroxyl groups in oligomer I is located at distances >1.5 nm away (the integral from 0 to ~6.0 nm is the same for all oligomers). The proximity of OH groups to $Si(OMe)_3$ groups indicates the steric possibility to form ether cross-links (Figure 1b). The area under the curve near ~1.2 nm therefore suggests that the density of cross-links may be higher in the order III~IV > I, showing a preference for polymer/oligomers that contain a larger number of OH-terminated side chains.

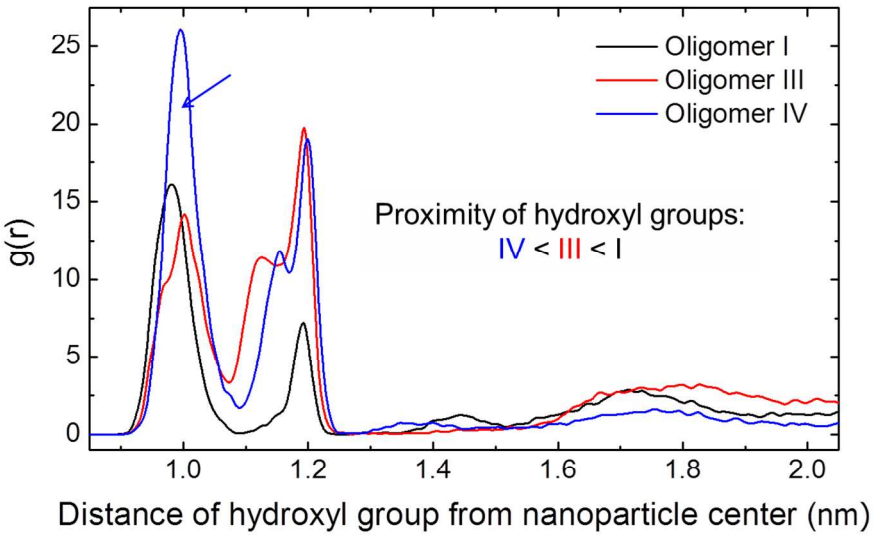

Figure 3. Radial distribution function of hydroxyl groups in oligomers I, III, and IV from the center of the nanoparticle. The area under the curve within a given distance interval is proportional to the probability of finding the OH group. Close approaches to the particle core and to the $Si(OMe)_3$ groups in the surfactant layer are seen near 1.0 nm and 1.2 nm, respectively. Oligomer IV approaches the particle core (arrow) most closely while oligomer III best approaches potentially reactive $Si(OMe)_3$ groups in the surfactant corona.

The distribution of ester groups in oligomers I, II, and III differs from that of the hydroxyl groups. The closest approach is 1.3 nm for a small fraction of oligomer III, which contains only one side chain per monomer. A significant presence of ester groups starts at 1.7-1.8 nm distance for all oligomers including oligomer III. This position is outside the MPS corona and reflects the steric unavailability of the ester group to the nanoparticle surface: it is attached to the rigid backbone on the carbonyl end and shielded by the undecyl chain on the alcohol end (Figure 1c).

In comparison, the ester group of oligomer III is closest to the nanoparticle, followed by oligomers II, I, and covalently attached oligomer I. Oligomers II and I are sterically challenged by the large alkoxy side chains to approach the surface closely. The side chains wrap around the surfactant corona and prevent the approach of the ester group. The ester groups are also significantly distributed over the distance range from 1.7 to more than 3.0 nm for all polymers. The lack of close approach to trimethoxysilyl groups at 1.2 nm distance also suggests that ester groups cannot achieve covalent attachment to the CdS-MPS nanoparticles via trans-esterification. The radial distribution function of the ester groups was also specifically tested for oligomer I with covalent bonds to the nanoparticles via the hydroxyl group (Figure 4). The position of the first peak and the rest of the distribution of the ester group are similar to non-covalently bonded oligomer I. Therefore, the interfacial structure may not be strongly modified even after covalent links are formed.

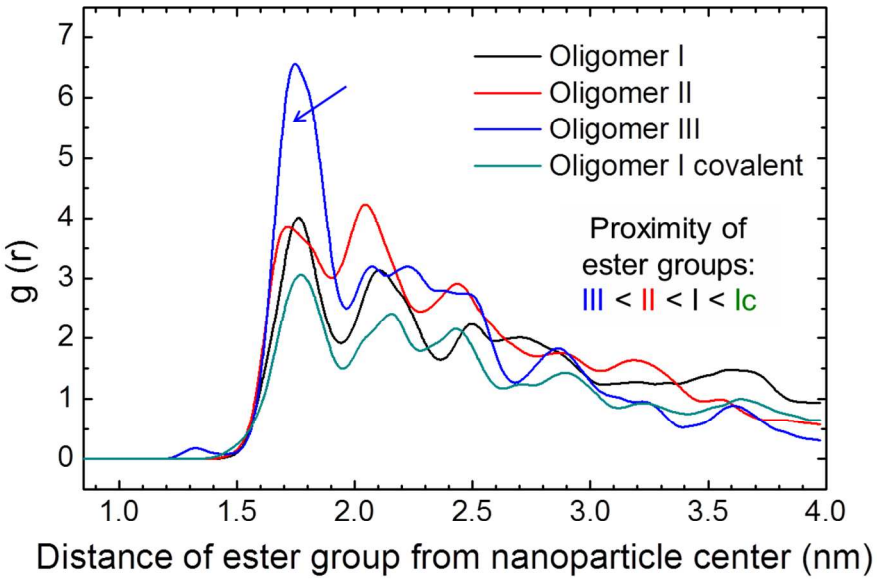

Figure 4. Radial distribution function of ester groups in oligomers I, II, and III, from the center of the nanoparticle. The area under the curve is proportional to the probability of finding the ester group in a given distance interval. Ester groups are distributed over a distance range from 1.7 nm to beyond 3.0 nm and hardly approach the MPS corona. The closest approach is seen for oligomer III (arrow) and the least close approach for oligomer I with covalent ether bonds to MPS.

Another oligomer-specific measure is the end-to-end length of the backbone averaged over time and all 20 molecules in the simulation (Figure 5). Instantaneous visualizations (Figure 2) reveal that the stiffness along the main chains is considerable while some bending occurs on the scale of several nm. The average end-to-end distance and radius of bending increase in the order of oligomers III<(I, IV)<II. This trend suggests that oligomer III with less side chains is more prone to bending than the others and possibly associates better with the nanoparticle. Oligomer IV is less bendable and structurally very similar to oligomer III, only missing the ester group. Oligomers I and II with more side chains show higher bending resistance. Oligomer II exhibits the longest end-to-end distance, possibly related to the absence of the hydroxyl group, which may bind strongly to the nanoparticle surface and strain the backbone. Moreover, a larger standard deviation of the observed end-to-end length for oligomers III and IV indicates higher bending fluctuations than in oligomers I and II. Stronger bending fluctuations are associated with the lower number of side chains and a higher rate of diffusion (D=2.3±0.6·10^{-5} cm^{2}s^{-1} for both oligomers III and IV) compared to oligomers I and II with more side chains and lower rate of diffusion (D=1.2±0.2·10^{-6} cm^{2}s^{-1} for oligomer I and D=4.6±0.9·10^{-7} cm^{2}s^{-1} for oligomer II). It is

emphasized that only relative diffusion coefficients can be compared at the reduced density while absolute values at full density are lower.

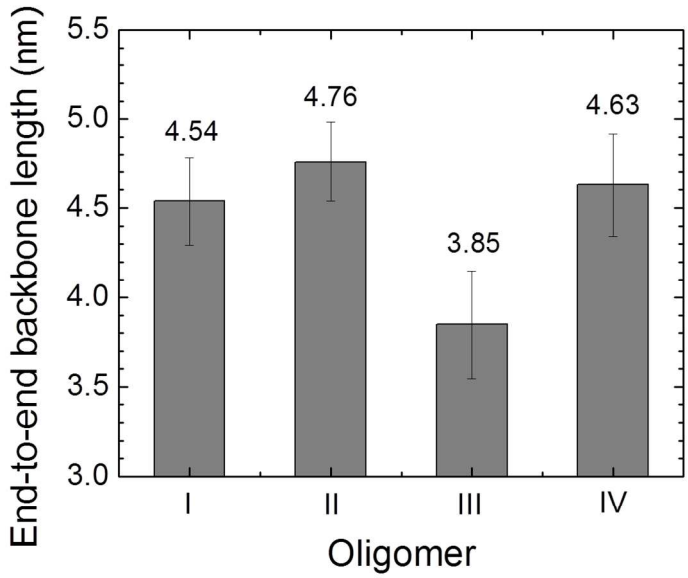

Figure 5. Average end-to-end distance of the oligomer backbones and standard deviation in molecular dynamics simulation. Lower values, especially for oligomer III, indicate bending of the linear molecular geometry.

4. Conclusions

Classical molecular dynamics simulation was employed to examine the interfacial structure and dynamics of several substituted poly(phenyleneethynylene) oligomers in contact with surfactant-modified cadmium sulfide nanoparticles. New force field parameters for CdS were introduced, consistent with the polymer consistent force field, and four different oligomers were investigated in contact with CdS modified with 3-mercaptopropyltrimethoxysilane (MPS) ligands. Terminal

hydroxyl groups on the side chains of the oligomers were found to penetrate the shell of the nanoparticles and coordinate core Cd^{2+} and S^{2-} ions through dipolar interactions. The hydroxyl groups are available for potential reaction with methoxysilane groups in the ligand corona to form silyl ether links. In contrast, sterically less available ester groups attached to the backbone were found unlikely to approach the ligand shell for trans-esterification. The presence of long side chains in the oligomer allowed wrapping onto the nanoparticle surface, reduced bending of the oligomer backbone, and slowed down the mobility of oligomers at the interface up to two orders of magnitude compared to oligomers with less alkyl content. Differences in interfacial structure between covalently cross-linked nanoparticle-polymer interfaces (via a terminal hydroxyl group) to that of non-covalently associated interfaces were not found to be significant. Simplifications in chain length and packing were necessary for computational feasibility; however, the results provide new perspectives on polymer dynamics at the surface of quantum dots. Further studies may examine specific ligand packing and the role of covalent attachment of polymers to moderate interactions between the nanoparticles in comparison with measurements.

Acknowledgements

We are grateful for support from the U.S. Air Force Office of Scientific Research and CONACyT through the joint U.S.-Mexico Basic Research Initiative, supported by AFOSR (FA9550-10-1-0236) and CONACyT (1010/189/10C-286-10). We acknowledge further support from Centro de Investigación en Quimica Aplicada (CIQA), Saltillo, Mexico, the University of Akron, Ohio, and the Ohio Supercomputing Center for the allocation of computational resources.

References

1. F. Ulrich and W. Zachariasen, *Zeit. Krist.*, 1925, 62, 260-273.
2. W. Mueller and G. Loeffler, *Angew. Chem.*, 1933, 46, 538-539.
3. W. O. Milligan, *J. Phys. Chem.*, 1934, 38, 797-800.
4. D. L. Klein, R. Roth, A. K. L. Lim, A. P. Alivisatos and P. L. McEuen, *Nature*, 1997, 389, 699-701.
5. Y. F. Chen and Z. Rosenzweig, *Analyt. Chem.*, 2002, 74, 5132-5138.
6. Y. Fang, L. Chen, C.-F. Wang and S. Chen, *J. Polym. Sci. a-Polym. Chem.*, 2010, 48, 2170-2177.
7. M. P. Espe, S. Y. Ortiz-Colon, A. Ponce and R. F. Ziolo, in *Advanced Electron Microscopy and Nanomaterials*, eds. A. Ponce and D. Bueno, 2010, vol. 644, pp. 123-127.
8. S. Masala, S. Del Gobbo, C. Borriello, V. Bizzarro, V. La Ferrara, M. Re, E. Pesce, C. Minarini, M. De Crescenzi and T. Di Luccio, *J. Nanopart. Res.*, 2011, 13, 6537-6544.
9. S. Dowland, T. Lutz, A. Ward, S. P. King, A. Sudlow, M. S. Hill, K. C. Molloy and S. A. Haque, *Adv. Mater.*, 2011, 23, 2739-2744.
10. B. Lama, *Synthesis and Characterization of CdS Nanoparticle/Polymer Composites*, University of Akron, PhD thesis, 2013, http://rave.ohiolink.edu/etdc/view?acc_num=akron1375797236.
11. Z. Fang, X. C. Wang, H. C. Wu and C. Z. Zhao, *Int. J. Photoener.*, 2011, DOI: 10.1155/2011/297350, 297350.
12. X.-Y. Yu, B.-X. Lei, D.-B. Kuang and C.-Y. Su, *Chem. Sci.*, 2011, 2, 1396-1400.
13. M. A. Hossain, J. R. Jennings, C. Shen, J. H. Pan, Z. Y. Koh, N. Mathews and Q. Wang, *J. Mater. Chem.*, 2012, 22, 16235-16242.
14. Y. Wang, N. Peng, H. Li and X. Bai, *J. Nanomater.*, 2012, DOI: 10.1155/2012/858693.
15. T. Torimoto, J. P. Reyes, S. Y. Murakami, B. Pal and B. Ohtani, *J. Photochem. Photobiol. a-Chem.*, 2003, 160, 69-76.
16. S. F. Wuister and A. Meijerink, *J. Luminesc.*, 2003, 102, 338-343.
17. Y. J. Eo, J. H. Kim, J. H. Ko and B. S. Bae, *J. Mater. Res.*, 2005, 20, 401-408.
18. Y. J. Eo, T. H. Lee, S. Y. Kim, J. K. Kang, Y. S. Han and B. S. Bae, *J. Polym. Sci. B-Polym. Phys.*, 2005, 43, 827-836.
19. H. Lee, H. C. Leventis, S.-J. Moon, P. Chen, S. Ito, S. A. Haque, T. Torres, F. Nueesch, T. Geiger, S. M. Zakeeruddin, M. Graetzel and M. K. Nazeeruddin, *Adv. Funct. Mater.*, 2009, 19, 2735-2742.
20. J.-S. Kim, S. Yang and B.-S. Bae, *J. Sol-Gel Sci. Tech.*, 2010, 53, 434-440.
21. M. Haase and A. P. Alivisatos, *J. Phys. Chem.*, 1992, 96, 6756-6762.
22. M. G. Berrettini, G. Braun, J. G. Hu and G. F. Strouse, *J. Am. Chem. Soc.*, 2004, 126, 7063-7070.
23. R. Elbaum, S. Vega and G. Hodes, *Chem. Mater.*, 2001, 13, 2272-2280.
24. V. Ladizhansky, G. Hodes and S. Vega, *J. Phys. Chem. B*, 1998, 102, 8505-8509.
25. V. Ladizhansky, G. Hodes and S. Vega, *J. Phys. Chem. B*, 2000, 104, 1939-1943.
26. J. S. Owen, J. Park, P.-E. Trudeau and A. P. Alivisatos, *J. Am. Chem. Soc.*, 2008, 130, 12279-12281.
27. A. J. Morris-Cohen, M. Malicki, M. D. Peterson, J. W. J. Slavin and E. A. Weiss, *Chem. Mater.*, 2013, 25, 1155-1165.
28. H. Heinz, R. A. Vaia and B. L. Farmer, *Langmuir*, 2008, 24, 3727-3733.

29. E. Arias-Marin, J. Le Moigne, T. Maillou, D. Guillon, I. Moggio and B. Geffroy, *Macromolecules*, 2003, 36, 3570-3579.
30. G. Castruita, E. Arias, I. Moggio, F. Perez, D. Medellin, R. Torres, R. Ziolo, A. Olivas, E. Giorgetti and M. Muniz-Miranda, *J. Mol. Struct.*, 2009, 936, 177-186.
31. G. Castruita, V. Garcia, E. Arias, I. Moggio, R. Ziolo, A. Ponce, V. Gonzalez, J. E. Haley, J. L. Flikkema and T. Cooper, *J. Mater. Chem.*, 2012, 22, 3770-3780.
32. R. J. Traill and R. W. Boyle, *Am. Miner.*, 1955, 40, 555-559.
33. B. J. Skinner, *Am. Mineral.*, 1961, 46, 1399-1411.
34. P. Klocek, *Handbook of Infrared Optical Materials*, Marcel Dekker, New York, 1991.
35. Y. T. Fu and H. Heinz, *Chem. Mater.*, 2010, 22, 1595-1605.
36. H. Heinz, R. A. Vaia and B. L. Farmer, *J. Chem. Phys.*, 2006, 124, 224713.
37. R. K. Mishra, R. J. Flatt and H. Heinz, *J. Phys. Chem. C*, 2013, 117, 10417-10432.
38. H. Heinz, T.-J. Lin, R. K. Mishra and F. S. Emami, *Langmuir*, 2013, 29, 1754-1765.
39. H. Heinz and U. W. Suter, *J. Phys. Chem. B*, 2004, 108, 18341-18352.
40. H. Heinz, H. J. Castelijns and U. W. Suter, *J. Am. Chem. Soc.*, 2003, 125, 9500-9510.
41. J. E. Huheey, E. A. Keiter and R. L. Keiter, *Inorganic Chemistry - Principles of Structure and Reactivity*, Harper Collins College Publishers, New York, 4th edn., 1993.
42. *Materials Studio 6.0 Program Suite and User Guide*, Accelrys, Inc., 2012.
43. H. Sun, S. J. Mumby, J. R. Maple and A. T. Hagler, *J. Am. Chem. Soc.*, 1994, 116, 2978-2987.
44. *CRC Handbook of Chemistry and Physics* CRC Press, Boca Raton, FL, 89th, Lide, D. R., edn., 2008.
45. S. Plimpton, *J. Comput. Phys.*, 1995, 117, 1-19.
46. H. Heinz, H. Koerner, K. L. Anderson, R. A. Vaia and B. L. Farmer, *Chem. Mater.*, 2005, 17, 5658-5669.
47. H. Heinz, R. A. Vaia, B. L. Farmer and R. R. Naik, *J. Phys. Chem. C*, 2008, 112, 17281-17290.
48. S. V. Patwardhan, F. S. Emami, R. J. Berry, S. E. Jones, R. R. Naik, O. Deschaume, H. Heinz and C. C. Perry, *J. Am. Chem. Soc.*, 2012, 134, 6244-6256.
49. L. Ruan, H. Ramezani-Dakhel, C.-Y. Chiu, E. Zhu, Y. Li, H. Heinz and Y. Huang, *Nano Lett.*, 2013, 13, 840-846.
50. D. Frenkel and B. Smit, *Understanding Molecular Simulation from Algorithms to Applications* Academic Press, San Diego, 2nd edn., 2002.

Graphical Abstract